Michail Manolidis[1]
Department of Biomedical Engineering,
University of Michigan,
Ann Arbor, MI 48109;
Laboratoire de Physique de la Matière
Condensée,
Ecole Polytechnique, CNRS,
Université Paris-Saclay,
Palaiseau Cedex 91128, France
e-mail: mihalis@umich.edu

Daniel Isabey
Professor
Inserm, U955 (Equipe13) and CNRS ERL 7240,
Cell and Respiratory Biomechanics,
Université Paris Est,
Créteil 94010, France
e-mail: daniel.isabey@inserm.fr

Bruno Louis
Inserm, U955 (Equipe13) and CNRS ERL 7240,
Cell and Respiratory Biomechanics,
Université Paris Est,
Créteil 94010, France
e-mail: bruno.louis@inserm.fr

James B. Grotberg
Professor
Department of Biomedical Engineering,
University of Michigan,
Ann Arbor, MI 48109
e-mail: grotberg@umich.edu

Marcel Filoche
Professor
Laboratoire de Physique de la Matière
Condensée,
Ecole Polytechnique, CNRS,
Université Paris-Saclay,
Palaiseau Cedex 91128, France;
Inserm, U955 (Equipe13) and CNRS ERL 7240,
Cell and Respiratory Biomechanics,
Université Paris Est,
Créteil 94010, France
e-ail: marcel.filoche@polytechnique.edu

A Macroscopic Model for Simulating the Mucociliary Clearance in a Bronchial Bifurcation: The Role of Surface Tension

The mucociliary clearance in the bronchial tree is the main mechanism by which the lungs clear themselves of deposited particulate matter. In this work, a macroscopic model of the clearance mechanism is proposed. Lubrication theory is applied for thin films with both surface tension effects and a moving wall boundary. The flow field is computed by the use of a finite-volume scheme on an unstructured grid that replicates a bronchial bifurcation. The carina in bronchial bifurcations is of special interest because it is a location of increased deposition of inhaled particles. In this study, the mucus flow is computed for different values of the surface tension. It is found that a minimal surface tension is necessary for efficiently removing the mucus while maintaining the mucus film thickness at physiological levels. [DOI: 10.1115/1.4034507]

1 Introduction

The walls of the bronchial tree are covered by a very thin layer of a water-like serous fluid, the *periciliary liquid* (PCL), on top of which lies a thin layer of mucus which is a non-Newtonian fluid exhibiting shear thinning as well as strong elastic properties. The constant motion of this mucus layer carries trapped particular matter which are eventually expelled into the esophagus. This mechanism, called the *mucociliary escalator*, is one of the main mechanisms by which the lungs continuously clear themselves of inhaled particles. The mucus motion is induced by the coordinated beating of cilia embedded in the PCL. During an effective stroke of a cilium, its tip slightly penetrates the overlying mucus layer and propels it, possibly together with the circulating PCL underneath. The slight phase shift between each cilium and its neighbors generates back-propagating waves (with respect to the mucus motion) called *metachronal waves*. The standard frequency of the cilium oscillation has been measured at approximately 20 Hz in the upper respiratory tract of human subjects [1]. From animal studies, it was found that the oscillation frequency drops moving down the respiratory tree [2]. in vitro, cilia have been measured to beat at 12–15 Hz at body temperature [3].

The aim of this article is twofold: first, to present a macroscopic model of mucociliary transport in which the cilia motion is summarized as a wall boundary condition for the mucus transport, second, to use this model to investigate the mucus flow in the complicated geometry of a carina, for various values of the fluid properties. Only steady state is considered. Ciliary forcing is time-averaged and modeled as a prescribed wall velocity in a two-layered film. Circulating mucus (the top layer) is treated as a Newtonian fluid, which is valid in steady-state flow for a Maxwell fluid [4]. The bottom layer consists of a transitional fluid that separates the PCL from the more viscous mucus layer on the top and is modeled as a less viscous Newtonian fluid. Airflow interactions are not considered in the model. Generally, their role in mucociliary clearance under normal physiological conditions with no

[1]Corresponding author.
Manuscript received December 18, 2015; final manuscript received August 9, 2016; published online November 3, 2016. Assoc. Editor: Naomi Chesler.

coughing is considered small [5,6]. Furthermore, airflow speed is very low in the section of the tree that is modeled in this work. Gravity is neglected in the model based on the fact that the Bond number—the force of gravity relative to that of surface tension—is very small in the section of the lung considered in our study. The governing equations are derived from fluid mechanics first principles and dimensional analysis. They are solved numerically with the finite-volume method on a three-dimensional manifold, modeled as an unstructured triangular surface grid. A computer-aided drawing (CAD) model of a symmetric bifurcation is created and meshed, and the mucus flow field is solved for on that mesh.

The motivation for this work lies in the fact that so little is known about the nature of mucus flow in bronchial bifurcations. These loci are favored sites for increased deposition of particles by impaction [7,8] and are potential sites for the development of cancer [9]. Simultaneously, they are also saddle points of the geometry which may theoretically be the stagnation points of the mucus flow, hence sites of less efficient clearance. It is therefore important to determine whether these regions are characterized by a slower than average flow, and how the mucus properties affect its flow. This work aims at examining the driving forces governing the mucus flow field pattern in these regions.

2 A Brief Overview of the Previous Work

Most studies on mucociliary clearance involve microscopic modeling of ciliary beating and mucus flow. An early overview of the experimental and theoretical work on the topic can be found in Ref. [10], while a more recent overview of the existing models can be found in Ref. [11]. Discrete ciliary beating models were developed early on [12–14] to study the flow field induced by a beating cilium. Sanderson and Sleigh [15] also included the effect of penetration of the tip of the cilium into viscous mucus on the beating pattern. These models allowed a first assessment of the nature and amount of the propulsive forces generated by the beating cilia and opened the way for the development of mucociliary clearance models.

A class of models of the clearance mechanism consists of so-called "traction layer" models, whereby ciliary forcing takes the form of a volume force continuous in space. This type of modeling was first introduced by Keller [16] for the study of ciliated organisms, and later applied by Blake and Winet to mucociliary clearance [17] who developed a steady-state time-averaged model where mucus and the PCL layer are described as Newtonian fluids. More recently, Smith et al. [18] proposed an unsteady traction layer model with three layers, the mucus being described as a Maxwell fluid bilayer. A propulsive volume force was implemented for the bottom mucus layer and a resistive volume force for the PCL layer, whereby PCL flow was likened to a flow through a porous medium. In this model, forcing varies sinusoidally and originates from the ciliary tips penetrating the mucus layer while the PCL layer plays a resistive role. A model that did not implement the traction layer approach was that by Ross [19] who considered the viscoelastic properties of mucus but modeled the mucus–PCL interface as an impermeable wavy surface. Specifically, Ross used a nonlinear, time periodic Lagrangian wall particle (ciliary tip) model that resulted in a steady Eulerian component of wall velocity. Liron and Rozenson [20] modeled ciliary forcing as a series of propulsive impulses by the ciliary tips in the form of Delta functions, but did not consider the PCL layer. Recently, Mitran presented an extremely sophisticated submicroscopic finite-element model [21], where the cilia were modeled as deforming solid structures interacting with the surrounding fluid. The same author also presented a work on modeling mucins at a molecular level in order to derive the macroscopic rheological properties of mucus in the respiratory tree [22].

One of the few systemic models of mucociliary clearance was developed by Lee et al. [23]. It is a one-dimensional model intended to compute the clearance of particles from the bronchial tree. More recent attempts to systemically model the mucociliary clearance followed a stochastic approach [24,25]. A recent attempt [26] modeled mucus flow in bronchial bifurcations as Newtonian pipe flow through the space bounded by concentric cylinders. The authors concluded that the bifurcation regions contain areas of reduced clearance.

Our work marks the first attempt to model the mucus film free surface flow on a 3D manifold representing part of the bronchial tree, and the macroscopic approach that is followed can allow for systemic modeling in the future.

3 Methodology

3.1 Governing Equations. We consider a three-dimensional flow on a flat surface, composed of two thin layers of fluid with different viscosities. The top layer is thicker and more viscous, while the bottom layer, very thin and less viscous, represents the region of the mucus film where the ciliary tips penetrate. With respect to surface tension the two layers are treated as one fluid, so only the air–mucus interface is responsible for surface tension induced pressure gradients. The characteristic substrate length scale, L, is orders of magnitude larger than the characteristic film thickness, h, i.e., $\varepsilon = (h/L) \ll 1$. Lubrication theory is invoked [27], and the flow is governed by the Stokes equations

$$\mu\frac{\partial^2 u}{\partial z^2} - \frac{\partial p}{\partial x} = 0 \quad \text{and} \quad \mu\frac{\partial^2 v}{\partial z^2} - \frac{\partial p}{\partial y} = 0 \tag{1}$$

where a local coordinate system has been fitted so that the x–y plane is the plane of the flat surface, and u and v are the velocity components along that plane. The second derivatives $(\partial^2/\partial x^2)$ and $(\partial^2/\partial y^2)$ have been dropped in accordance to the lubrication theory, and so has the vertical velocity $w \ll u, v$. Two-dimensionless numbers characterize the flow: the Capillary number, $\mathrm{Ca} = (\mu U_o/\gamma)$, and the Bond number, $\mathrm{Bo} = h^2\rho g/\gamma$, where μ is the fluid viscosity, ρ is the fluid density, γ is the surface tension coefficient entering Laplace's law (see Eq. (4) below), g is the acceleration of gravity, and U_0 is the typical flow speed. Gravity is neglected in our study because the Bond number is of order 10^{-5} at the location of the bronchial tree that is considered. Figure 1 schematically shows the geometry, where the local coordinate system is such that the flow is parallel to the x–y plane, with components u_o and v_o for the bottom layer and u_m and v_m for the top layer.

The Stokes equations can be integrated to find the flow field in the two layers. The first round of integration is applied to the top layer in order to apply a zero-stress boundary condition at the air–mucus interface. This allows for the calculation of the shear stress at the interface between the two layers. Then, the bottom layer is integrated once, whereby the integration constant is computed from a force balance at the interface between the two layers. It is integrated again and, by applying a no-slip condition at the wall, the flow field for the bottom layer is resolved. Then, the top layer is integrated again, and the integration constant is computed by applying a no-slip boundary condition at the interface. The flow field at the top layer has now been resolved.

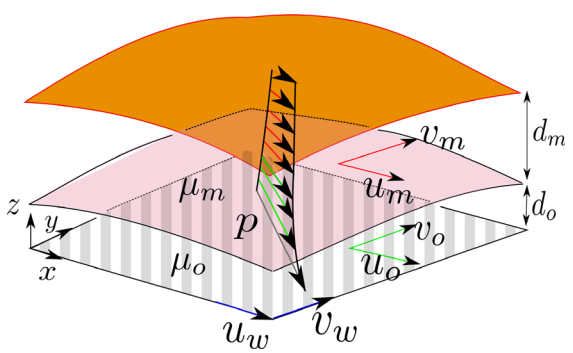

Fig. 1 Geometry of 3D two-layered flow on a flat plate

For the bottom layer ($0 \le z \le d_o$), the flow field is given by

$$u_o(x,y,z) = \frac{1}{\mu_o}\frac{\partial p}{\partial x}\left[\frac{z^2}{2} - (d_o + d_m)z\right] + u_w \tag{2}$$

and

$$v_o(x,y,z) = \frac{1}{\mu_o}\frac{\partial p}{\partial y}\left[\frac{z^2}{2} - (d_o + d_m)z\right] + v_w \tag{3}$$

where $u_w(x,y)$ and $v_w(x,y)$ are the prescribed wall velocity components, and μ_o is the viscosity of the bottom layer. d_o and $d_m(x,y)$ are the thicknesses of the bottom and top layer, respectively. The model assumes a constant thickness of the bottom layer, based on the experimental findings that show that the transition from the PCL to the mucus layers is sharply demarcated with little variation in thickness under physiological conditions [28]. Due to surface tension, a pressure jump occurs across the air–mucus interface. Setting the air pressure as the reference, the pressure p in the film is given by the Young–Laplace equation

$$p(x,y) = -2\gamma\ H(x,y) \tag{4}$$

where $H(x, y)$ is the mean curvature of the free surface

$$2H = -\nabla \cdot \hat{n} \tag{5}$$

This curvature is an invariant (independent of reference frame). $\hat{n}$ is the surface normal, and the convention is followed whereby it is positive when the mucus forms a convex free surface. From now on, by curvature we will refer to the mean curvature unless specified otherwise. The free surface curvature is computed numerically in the model.

For the top layer ($d_o < z \le d_o + d_m$), the flow field is

$$u_m(x,y,z) = \frac{1}{\mu_m}\frac{\partial p}{\partial x}\left(\frac{z^2}{2} - (d_o + d_m)z - \left(\frac{d_o^2}{2} + d_o d_m\right)\left(\frac{\mu_m}{\mu_o} - 1\right)\right) + u_w \tag{6}$$

and

$$v_m(x,y,z) = \frac{1}{\mu_m}\frac{\partial p}{\partial y}\left(\frac{z^2}{2} - (d_o + d_m)z - \left(\frac{d_o^2}{2} + d_o d_m\right)\left(\frac{\mu_m}{\mu_o} - 1\right)\right) + v_w \tag{7}$$

where μ_m is the viscosity of the top layer. The boundary conditions imposed when solving the Stokes equations are no slip at the bottom with a prescribed wall velocity, no slip at the interface between the two layers, zero shear on the free surface with a pressure jump due to surface tension, and force balance at the interface between the two layers.

The model proposed here merges the layers into one single compound layer. We can define for this compound layer the average velocity components, $\bar{u}$ and $\bar{v}$

$$\bar{u}(x,y) = \frac{1}{d_o + d_m}\left(\int_0^{d_o} u_o\ dz + \int_{d_o}^{d_o+d_m} u_m\ dz\right) \tag{8}$$

$$\bar{v}(x,y) = \frac{1}{d_o + d_m}\left(\int_0^{d_o} v_o dz + \int_{d_o}^{d_o+d_m} v_m dz\right) \tag{9}$$

Carrying out the integration over the entire thickness yields

$$\bar{u}(x,y) = -\frac{\partial p}{\partial x}\left(\frac{1}{\mu_m}\frac{d_m}{d_m + d_o}\left(\frac{1}{2}\frac{\mu_m}{\mu_o}d_o^2 + \frac{\mu_m}{\mu_o}d_m d_o + \frac{1}{3}d_m^2\right) + \frac{1}{\mu_o}\frac{d_o}{d_m + d_o}\left(\frac{d_o^2}{3} + \frac{d_m d_o}{2}\right)\right) + u_w \tag{10}$$

$$\bar{v}(x,y) = -\frac{\partial p}{\partial y}\left(\frac{1}{\mu_m}\frac{d_m}{d_m + d_o}\left(\frac{1}{2}\frac{\mu_m}{\mu_o}d_o^2 + \frac{\mu_m}{\mu_o}d_m d_o + \frac{1}{3}d_m^2\right) + \frac{1}{\mu_o}\frac{d_o}{d_m + d_o}\left(\frac{d_o^2}{3} + \frac{d_m d_o}{2}\right)\right) + v_w \tag{11}$$

where $\bar{u}$ and $\bar{v}$ are the depth-averaged horizontal velocity components. These quantities are functions of x and y since p, d_m, u_w, and v_w are all functions of x and y. The continuity equation writes

$$\frac{\partial u}{\partial x} + \frac{\partial v}{\partial y} + \frac{\partial w}{\partial z} = 0 \tag{12}$$

Integrating over the entire film thickness, $d_t (= d_o + d_m)$, gives

$$\frac{\partial}{\partial x}\int_0^{d_t} u\ dz - u|_{z=d_t}\frac{\partial d_t}{\partial x} + \frac{\partial}{\partial y}\int_0^{d_t} v\ dz - v|_{z=d_t}\frac{\partial d_t}{\partial y} + w|_{z=d_t} = 0 \tag{13}$$

where Leibniz's rule is used to take the derivative out of the integral of u and v, respectively. The vanishing flow normal to the free surface produces the following kinematic boundary condition

$$w|_{z=d_t} - \frac{\partial d_t}{\partial t} - u|_{z=d_t}\frac{\partial d_t}{\partial x} - v|_{z=d_t}\frac{\partial d_t}{\partial y} = 0 \tag{14}$$

The continuity equation then becomes

$$\frac{\partial d_t}{\partial t} + \frac{\partial (d_t \bar{u})}{\partial x} + \frac{\partial (d_t \bar{v})}{\partial y} = 0 \tag{15}$$

which can be rewritten in vector form as

$$\frac{\partial d_t}{\partial t} + \nabla_H \cdot (d_t \bar{\mathbf{u}}) = 0 \tag{16}$$

where $\nabla_H = (\partial/\partial x)\hat{i} + (\partial/\partial y)\hat{j}$ is the horizontal gradient operator, and $\bar{\mathbf{u}} = \bar{u}\hat{i} + \bar{v}\hat{j}$ is the horizontal average velocity vector. From now on, the mucus flow field and the flow speed refer to the depth (thickness)-averaged velocity and its magnitude, respectively (see Sec. 4). Equations (10), (11), and (16) form a system of three equations in three unknowns, $\bar{u}$, $\bar{v}$, and d_m.

3.2 Solution Methodology. The governing equations are solved numerically by implementing the finite-volume method. The geometric domain is broken up into piecewise flat areas (volumes), each of which we assume to have a constant mucus film thickness and on which flow is horizontally uniform. As will be detailed below, the curvature of the free surface is computed at the centroid of each flat triangular element from the film thickness at the centroids of neighboring triangles. Since the film thickness is very small compared to the physical domain, the curvature of the domain governs the free surface curvature. The two flow velocity Eqs. (10) and (11) can be written in the following vector form:

$$\bar{\mathbf{u}} = -\nabla p\left(\frac{1}{\mu_m}\frac{d_m}{d_m + d_o}\left(\frac{1}{2}\frac{\mu_m}{\mu_o}d_o^2 + \frac{\mu_m}{\mu_o}d_m d_o + \frac{1}{3}d_m^2\right) + \frac{1}{\mu_o}\frac{d_o}{d_m + d_o}\left(\frac{d_o^2}{3} + \frac{d_m d_o}{2}\right)\right) + \mathbf{u}_w = -B\ \nabla p + \mathbf{u}_w \tag{17}$$

where $\mathbf{u}_w$ is the wall velocity vector, and B corresponds to the algebraic expression in big parentheses. Integrating Eq. (17) over surface A of uniform film thickness and wall velocity (hence constant B), and applying the divergence theorem gives that area-average velocity

$$\bar{\mathbf{u}} = -\frac{1}{A}B\oint_{\partial A} p\ d\mathbf{S} + \mathbf{u}_w \tag{18}$$

where ∂A stands for the boundary of A. The discretized version of this equation writes

$$\bar{\mathbf{u}}_i = -\frac{1}{A_i}B\sum_{j=1}^{3} p_j l_j \mathbf{n}_j + \mathbf{u}_{iw} \tag{19}$$

where $\bar{\mathbf{u}}_i$ and $\mathbf{u}_{iw}$ are the average flow and wall velocities of element i, respectively, in the triangular area A_i, p_j is the pressure at side j of length l_j, and $\mathbf{n}_j$ is the outward normal. Integrating the average velocity continuity Eq. (16) over an area A with boundary ∂A, and applying the divergence theorem gives

$$\frac{\partial d_t}{\partial t} + \frac{1}{A}\oint_{\partial A} d_t \bar{\mathbf{u}} \cdot d\mathbf{S} = 0 \tag{20}$$

which becomes after discretization

$$\frac{\Delta d_t}{\Delta t} + \frac{1}{A_i}\sum_{j=1}^{3} d_{t,uw} u_j l_j = 0 \tag{21}$$

where $d_{t,uw}u_j l_j$ is the upwind flux of thickness $d_{t,uw}$ through side j. By picking an appropriate time step, Δt, the mucus film thickness is updated as follows:

$$\Delta d_t^{n+1} = \Delta d_t^n - \Delta t \frac{1}{A_i}\sum_{j=1}^{3} d_{t,uw} u_j l_j \tag{22}$$

where the superscript n indicates the n-th step. While upwinding is implemented for the film thickness, the fluxes at the edges are computed by interpolation.

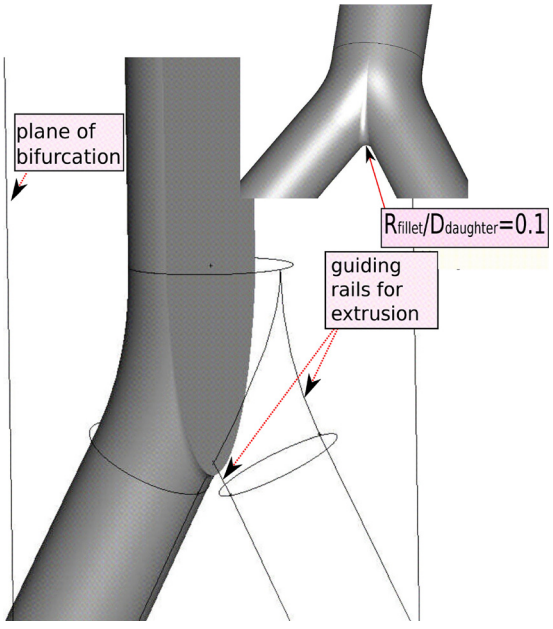

Fig. 2 Construction of a CAD model of a symmetric bifurcation

The solution scheme involves computing the flow field using an initial value for the film thickness d_t, then, updating this thickness from the flow field and the continuity equation. The process is repeated until a steady state is achieved. Every time the film thickness is updated, the free surface curvature has to be recomputed. Both the new film thickness and the new curvature enter the momentum equations when the flow field is updated. The value of the time step, Δt, is classically governed by the Courant–Friedrichs–Lewy (CFL) condition. However, the momentum equations are nonlinear in the film thickness, both in the computation of the free surface curvature and in the algebraic form of B in Eq (17). It was empirically found that Δt has to be smaller than the value allowed by the CFL condition.

The elements are taken to be orthogonal parallelepipeds and not trapezoidal wedges in profile. This incurs some numerical error in the film thickness estimation, which is relatively small compared to the inaccuracy of the numerical scheme implemented, and which becomes smaller with grid refinement.

3.3 Mass Conservation. The finite-volume method conserves mass locally, since at each iteration (time step) the film thickness of each element is adjusted based on the net influx of mass in that element. Simple inflow and outflow boundary conditions are imposed, and the film thickness at boundary cells is adjusted accordingly, and the mass is conserved globally. In the code that we have developed, we check that the mass is conserved throughout the computational domain at each iteration.

3.4 Geometric Model. The flow of mucus in a typical fifth generation bronchial bifurcation of an adult male is studied. To that end, a CAD model of a symmetric bifurcation is created, see Fig. 2, in accordance to Weibel's "A" symmetric model [29]. The branching angle between the daughter bronchi is 60 deg. The parent and one daughter bronchus are created as straight cylindrical segments. We employ the diameter, D_n, dependency on airway generation, n, as $D_n = D_0 \times 2^{-n/3}$ [30], where D_0 is the tracheal diameter. In our example, $D_0 = 2.5$ cm, and the parent tube is $n = 5$ while the daughters are $(n+1)$=6. One then morphs into the other trough "guiding rails,", which are splines constructed to avoid the sharp transitions/corners in the final model. The resulting volume is mirrored to itself on the sagittal plane, to produce a perfectly symmetric bifurcation. A fillet with the desired radius is then fitted in place of the edge that the two halves share. The final model is devoid of any sharp corners.

The most important geometric parameter of the model is the curvature ratio, that is, the minimum curvature radius at the center of the carina divided by the daughter branch diameter. As seen in the figure, it is given the value of 0.1, which is the average value based on anatomical findings [31]. In the geometric model, the diameter of the daughter bronchi is 7 mm, that of the parent bronchus is 8.82 mm, and the spur curvature radius in the plane of the bifurcation is 0.7 mm.

An unstructured triangular grid of the bifurcation is constructed. The free surface curvature is computed at the centroid of each triangle and is based on the location of the free surface in the three neighboring triangles. The methodology followed is similar to that described by Garimella and Swartz [32]. His method involved fitting a quadric of the form $z = ax^2 + bxy + cy^2$, where x, y, and z are the local coordinates of the free surface at the centroid of neighboring triangles, with the origin placed at the location of the free surface at the centroid of the central triangle. We find that the quadric fitted does not provide enough accuracy for our purposes. To achieve higher accuracy in curvature estimation we fit a fourth-order polynomial of the form $z = a_1x^4 + a_2x^3y + a_3x^2y^2 + a_4xy^3 + a_5y^4 + a_6x^3 + a_7x^2y + a_8xy^2 + a_9y^3 + a_{10}x^2 + a_{11}xy + a_{12}y^2 + a_{13}x + a_{14}y + a_{15}$. Many neighboring points are used for fitting the curve. When the number of points exceeds the number of constants, a least squares approach is followed. The mean curvature is computed analytically from the formula

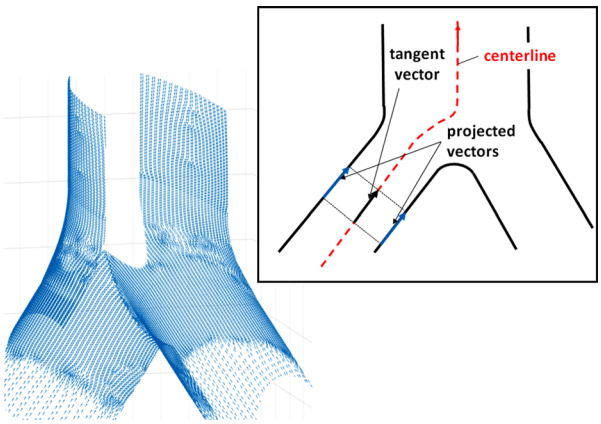

Fig. 3 Assigned wall velocity field showing the ridge region. Note: The vectors all have the same magnitude corresponding to a speed of 40 μm/s.

$$2H = \frac{\left(1+\left(\frac{\partial z}{\partial x}\right)^2\right)\frac{\partial^2 z}{\partial y^2} - 2\frac{\partial z}{\partial x}\frac{\partial z}{\partial y}\frac{\partial^2 z}{\partial x \partial y} + \left(1+\left(\frac{\partial z}{\partial y}\right)^2\right)\frac{\partial^2 z}{\partial x^2}}{\left(1+\left(\frac{\partial z}{\partial x}\right)^2+\left(\frac{\partial z}{\partial y}\right)^2\right)^{\frac{3}{2}}} \tag{23}$$

The curvature in the dividing spur region is strongly negative while it is positive elsewhere. The gradient in curvature causes a gradient in surface tension induced pressure.

The polynomial-fitting procedure outlined is performed at each time step/iteration for each element. That is, the curvature at the centroid of each element is computed at each time step, since the film thickness changes with each iteration.

A wall velocity field is proposed to model the direction and magnitude of ciliary forcing. The direction of the wall velocity vector in each planar element is set by projecting the unit vector tangent to the centerline onto this element (inset in Fig. 3). The wall velocity magnitude is set equal to 40 μm/s in the entire domain, a value consistent with experimental findings [33,34]. In fact, the value used in our model might be a slight overestimate according to the recent stochastic models which assign a smaller value to mucus flow speed in a fifth generation bifurcation [35]. Note that the lower mucus flow speed allows for surface tension to have a more pronounced effect. The resulting wall velocity field in the ridge region is also depicted in Fig. 3. In the absence of any precise knowledge of the cilia motion in the region of the carina, this type of velocity field is the simplest and strongest assumption. The influence of the underlying cilia forcing on the resulting mucus velocity field will be the subject of future studies.

While the prescribed wall velocity is symmetric analytically with respect to the plane of the bifurcation and the sagittal plane, the grid is unstructured triangular and is not perfectly symmetric. As such, the streamlines at the ridge in Fig. 3 are not perfectly straight. Artifacts from the plotting software used (MATLAB) may also affect the appearance of the streamlines in the figure. The effect that these unwanted asymmetries may have is not important in our opinion, since perfect symmetry is a rare find in nature herself.

Figure 4 shows the streamlines of the prescribed wall velocity field in the region of the carina. It can be seen that flow converges to the centerline of the ridge from both sides comprising the inner walls of the daughter bronchi, and the mucus is drained toward the anterior and posterior walls of the parent bronchus along the ridge.

The inflow and outflow boundary conditions at each extremity of the bifurcation are the following: a zero pressure gradient in the axial direction is set at the outflow, while the upstream total mucus film thickness at the inflows is set to 7 μm, which is within the physiologically observed values [36]. The bottom layer thickness is set to a constant value of 0.5 μm, in accordance with the published observations [36]. Using values that are based on the rheological studies [10,37], viscosity of bottom and top mucus film layers are set to 6 and 48 times the viscosity of water, respectively (0.006 Pa·s and 0.048 Pa·s). Assigning a fixed value to respiratory mucus viscosity is based on the time-averaged, steady-state approach that is followed, since it is actually a non-Newtonian fluid with shear-thinning properties. The coefficients of surface tension for our simulations are 0.0024, 0.0048, 0.0096, and 0.0192 N·m^{-1}. Physiologic airway surface tensions are represented by the highest value [10,38,39]. While the lower values are realized in alveoli [40], for airways they may better reflect the passage and deposition of surfactant during surfactant replacement therapy [41]. This range serves the purpose of elucidating the role of surface tension. Finally, surface tension is assumed to be uniform throughout the bifurcation. We thus neglect here the possible existence of surface tension gradients induced by the presence of surfactant pulled from the alveolar region by Marangoni effects and ciliary transport [42–44].

4 Results

The simulations were run on a grid comprised of 45,208 elements. This level of refinement was found adequate for physically meaningful and computationally accurate results. Finer grids were tested and the difference between maximum values of mucus film thickness did not exceed 5%. Figure 5 shows a contour plot of the pressure distribution in the ridge region. One can observe a strong

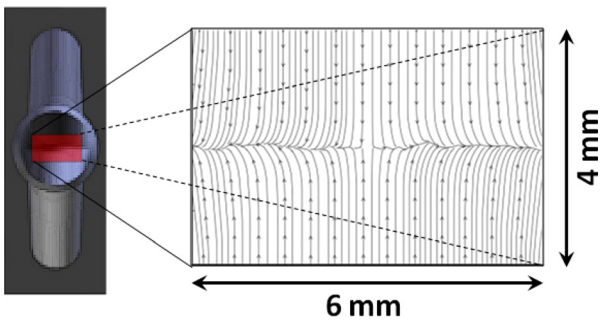

Fig. 4 Streamlines of the prescribed wall velocity field at the ridge. The zoomed region is a rectangle following the bifurcation wall, centered across the ridge, of curvilinear length and with 6 mm and 4 mm, respectively. The carina is the center of the rectangle.

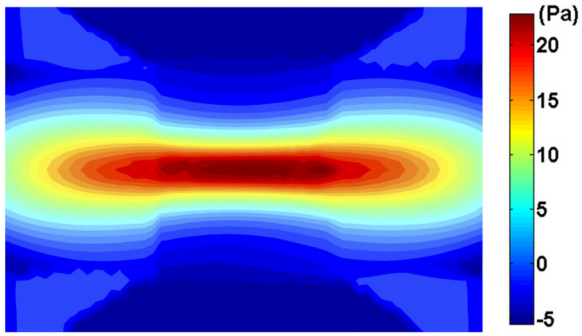

Fig. 5 Contour plot of the pressure along the ridge (the rectangle area is identical to the one delimited in Fig. 4). The sharp drop over small distances signals a strong pressure gradient (Ca = 10^{-4}).

pressure gradient due to the curvature gradient that directs mucus away from the ridge.

Figure 6 shows the streamlines of the mucus flow field (under steady state) in the dividing region for four different values of the capillary number ($\mathrm{Ca} = (\mu_m U_o/\gamma)$), where the magnitude of the prescribed wall velocity, 40 μm/s, is chosen as the characteristic velocity, U_o. The capillary number is adjusted by changing the value of surface tension, γ. From now on, the mucus flow field and flow speed are thickness-averaged quantities. One can see in the figure that surface tension dramatically alters the characteristics of the mucus flow field in the ridge region. Without surface tension, the flow field and the wall velocity field would coincide, and the streamlines would be identical to those of Fig. 4. Two salient features emerge from Fig. 6. First, the flow originated from each quadrant of a daughter bronchus is diverted toward the anterior and posterior walls of the parent bronchus by the action of surface tension. Second, the flow field is not symmetric with respect to the plane of bifurcation, but appears to possess rotational symmetry of order 2 (i.e., invariant by a rotation of 180 deg about the axis of the parent bronchus). This feature is more pronounced for smaller capillary numbers. Numerous simulations have been run, with different geometries and various levels of grid refinement. This symmetry feature has always been present, which leads to think that this configuration is selected by the system as a more stable one.

Figure 7 shows contour plots of flow velocity magnitude in the ridge region for the same four values of the capillary number. In addition to rotational symmetry of order 2, another feature is that for smaller capillary numbers, the flow speeds are larger along the ridge (stronger surface tension). Weakening the surface tension has a depressing effect on the flow speeds. For $\mathrm{Ca} = 10^{-4}$, which is the most realistic value used, the flow speed drastically increases in some areas, reaching about three times the wall velocity magnitude. Furthermore, there appear to be two diametrically opposed pathways—similar to "conveyor belts"—that clear mucus from the saddle point at speeds significantly higher than the wall velocity magnitude (light colors in the figure). Overall, the flow speed never drops below half the wall velocity magnitude anywhere in the domain. This can be compared to the case where surface tension is the weakest ($\mathrm{Ca} = 8 \times 10^{-4}$), whereby flow speeds are less than the wall velocity magnitude almost throughout the entire area of interest. This very low value of the surface tension is normally not encountered in physiological condition, but is chosen here to fully investigate the interplay between forcing and surface tension.

When plotting the film thickness in the entire bifurcation (Fig. 8), one can observe that it is uniform in the straight segments (as the flow field), except near the bifurcation region, much closer than a distance of three diameters. This is important because the length-to-diameter ratio for bronchial segments is $L/D \approx 3$, which is considered standard for mammalian lungs [7], and setting a uniform film thickness at the inflows as a boundary condition is, thus, appropriate. The mucus film is thicker at the outlet by an amount consistent with global mass conservation.

Figure 9 shows contour plots of the mucus film thickness at the ridge region for the same aforementioned capillary numbers. For higher capillary numbers, one can observe a significant thickening of the mucus film. Mathematically, flow conservation tells us that this thickening is correlated to the slow flow speeds observed earlier (Fig. 7). Physiologically, surface tension appears to play two different but correlated roles. It mitigates mucus film thickening at the ridge and it expedites clearance of mucus from the vicinity of the saddle point. Surface tension seems to play a vital role in the creation of a pathway—a conveyor belt of sorts—which clears mucus rapidly from the ridge region; these pathways are the two branches seen in Fig. 7. The transport of mucus from the daughter branches to the ridge region requires the cilia to work against a pressure gradient. Energy is being pumped into the system and stored as potential energy due to surface-tension-induced fluid pressure. Surface tension also modulates the flow dynamics by creating the conveyor belt mechanism by which mucus is cleared from the central area at speeds higher than those allowed by ciliary beating alone, by directing the release of the energy stored in the form of potential energy.

5 Discussions

Based on the findings of the model, we conclude that the surface tension speeds up clearance of mucus from the saddle point vicinity, and prevents excessive accumulation of mucus at the carinal ridge of bronchial bifurcations. As expected, surface tension is influential where curvatures are large. When realistic values for the surface tension coefficient are used, flow speeds can exceed three times the magnitude of the wall velocity at certain locations. At the same time, the flow field exhibits a rotational symmetry of order 2. In this configuration, two diametrically opposed and slightly spiraling pathways drain mucus from the saddle point area at very high speeds. This "conveyor belt" mechanism is powered by the force of surface tension and potential energy stored in the free surface. We note, however, that the computed flow patterns are to a certain extent the result of the assumption of a constant wall velocity magnitude. Experimental data revealing actual flow patterns in this region are highly awaited. We are also working toward incorporating porosity effects to our model, in which case the wall velocity will not have a fixed magnitude.

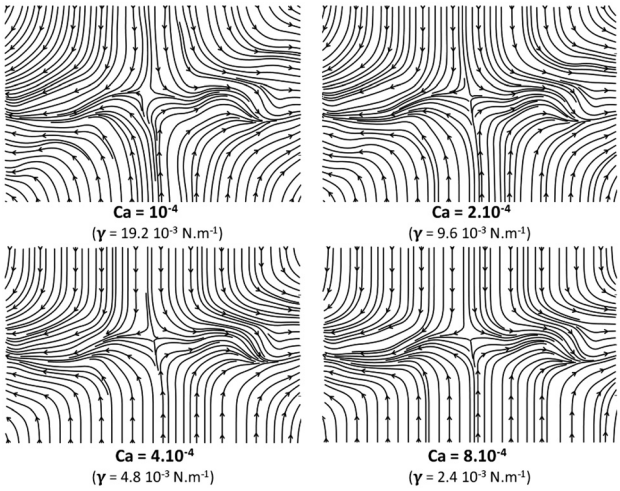

Fig. 6 Streamlines of the mucus flow field at the ridge region for four different capillary numbers (the rectangle area is identical to the one delimited in Fig. 4).

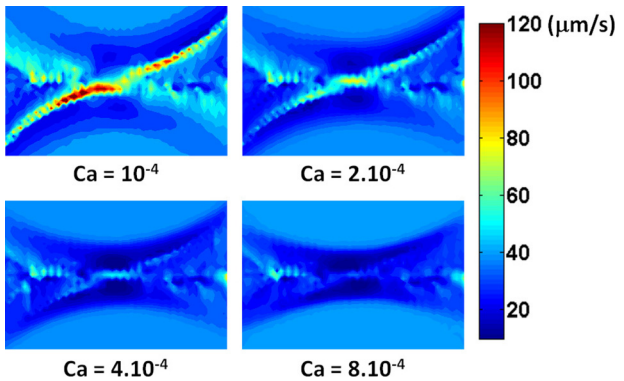

Fig. 7 Contour plots of flow velocity magnitude in the ridge region (the rectangle area is identical to the one defined in Fig. 4).

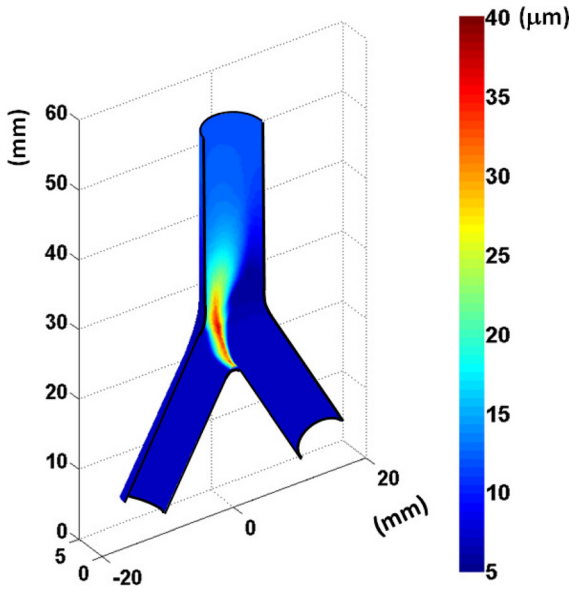

Fig. 8 Three-dimensional representation of the mucus thickness in the entire bifurcation, for $Ca = 8 \times 10^{-4}$. One can observe that the thickness stabilizes to a constant value far from the bifurcations, in all three branches.

The chosen magnitude of the prescribed wall velocity is based on findings of studies of mucus flow in the first bronchial generations [35,45]. Mucus flow velocities are lower at smaller bronchi while the curvature gradient is inversely proportional to the square of the diameter; the smaller the bronchi the greater the role of surface tension in modulating flow at bifurcations. Furthermore, if there are discontinuities in the mucus film layer, as may happen [10], the role of surface tension could be even greater, since in such regions less viscous underlying fluid would be exposed. Conditions that lead to an increase in mucus viscosity, on the other hand, such as chronic obstructive pulmonary disease (COPD) and cystic fibrosis (CF), will compromise the role of surface tension in clearing mucus from bifurcations. Tipping the force balance toward the side of viscosity will cause excessive accumulation of near-stagnating mucus in the carinal ridge. This would expose this area to bacterial infection as well as prolong the effects of toxins. Finally, certain substances, namely vaporized PFCs, can significantly alter the balance between surface tension and viscous forces, and may have an effect in mucus clearance in bifurcations.

In terms of the model itself, it is not clear whether it is best to model the ciliary beating as a prescribed wall velocity or as a volume force that acts on the bottom layer. The latter is the basis of traction layer models developed in the past [16–18]. We follow the former approach; the exact mechanics of mucus propulsion are still not clear and we base our approach on the premise that PCL fluid circulation generates movement on the overlying mucus layer. Our approach allows for a straightforward computational solution, and the validity of our conclusions with respect to the role of surface tension is not compromised. Furthermore, the film is modeled as a bilayer, without the need to explicitly take into account the PCL layer. Both layers comprising the film are taken to be Newtonian fluids, due to the chosen macroscopic time-averaged approach. Incorporating visco-elastic effects is, however, an important next step in the evolution of the model.

In conclusion, a key mechanism is proposed by which mucus flow in bronchial bifurcations, specifically in the carinal ridge region, is modulated. Surface tension acts to expedite the clearance of mucus (and trapped debris) from that area, which physiologically is an area of increased particle deposition. An implication is that agents or conditions that affect the strength of surface tension in the RT may have a profound effect in the ability of the lungs to clear themselves of inhaled matter or administered drugs in the form of aerosols.

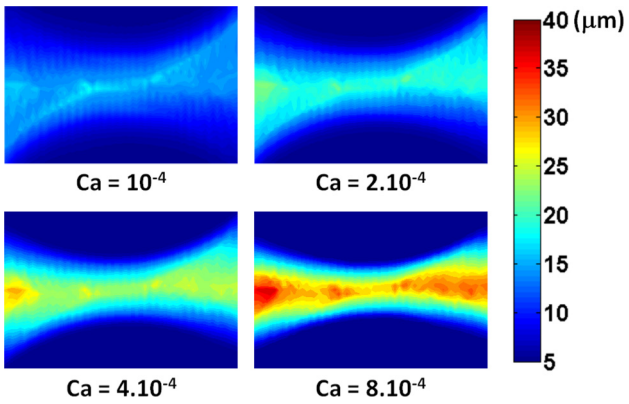

Fig. 9 Contour plots comparing film thickness at the ridge region for four different capillary numbers (the rectangle area is identical to the one defined in Fig. 4

References

[1] Reimer, A., von Mecklenberg, C., and Toremalm, N. G., 1978, "The Mucociliary Activity of the Upper Respiratory Tract III. A Functional and Morphological Study on the Human and Animal Material With Special Reference to Maxillary Sinus Diseases," Acta Otolaryngol., **355**, pp. 1–20.

[2] Iravani, J., 1967, "Flimmerbewegung in den Intrapulmonalen Luftwegen der Ratte," Pflugers Arch., **297**(4), pp. 221–237.

[3] Salathe, M., 2007, "Regulation of Mammalian Ciliary Beating," Annu. Rev. Physiol., **69**(1), pp. 401–422.

[4] Lai, W. M., Rubin, D., and Krempl, E., 2009, *Introduction to Continuum Mechanics*, Elsevier, Waltham, MA.

[5] Blake, J. R., 1975, "On the Movement of Mucus in the Lung," J. Biomech., **8**(3–4), pp. 179–190.

[6] Mauroy, B., Fausser, C., Pelca, D., Merck, J., and Flaud, P., 2011, "Toward the Modeling of Mucus Draining From the Human Lung: Role of the Geometry of the Airway Tree," Phys. Biol., **8**, p. 056006.

[7] de Vasconcelos, T. F., Sapoval, B., Andrade, J. S., Grotberg, J. B., Hu, Y., and Filoche, M., 2011, "Particle Capture in the Lung Made Simple?," J. Appl. Physiol., **110**(6), pp. 1664–1673.

[8] Kleinstreuer, C., Zhang, Z., and Li, Z., 2008, "Modeling Airflow and Particle Transport/Deposition in Pulmonary Airways," Respir. Physiol. Neurobiol., **163**(1), pp. 128–138.

[9] Balashazy, I., Hofmann, W., and Heistracher, T., 2003, "Local Particle Deposition Patterns may Play a Key Role in the Development of Lung Cancer," J. Appl. Physiol., **94**(5), pp. 1719–1725.

[10] Sleigh, M. A., Blake, J. R., and Liron, N., 1988, "The Propulsion of Mucus by Cilia," Am. Rev. Respir. Dis., **137**(3), pp. 726–741.

[11] Smith, D. J., Gaffney, E. A., and Blake, J. R., 2008, "Modelling Mucociliary Clearance," Respir. Physiol. Neurobiol., **163**(1), pp. 178–188.

[12] Blake, J. R., 1972, "A Model for the Microstructure in Ciliated Micro-Organisms," J. Fluid Mech., **55**(01), pp. 1–23.

[13] Liron, N., and Mochon, S., 1976, "The Discrete Cilia Approach to Propulsion of Ciliated Microorganism," J. Fluid Mech., **75**(03), pp. 593–607.

[14] Fulford, G. R., and Blake, J. R., 1986, "Muco-Ciliary Transport in the Lung," J. Theor. Biol., **121**(4), pp. 381–402.

[15] Sanderson, M. J., and Sleigh, M. A., 1981, "Ciliary Activity of Cultured Rabbit Tracheal Epithelium: Beat Pattern and Metachrony," J. Cell Sci., **47**, pp. 331–347.

[16] Keller, S. R., 1975, "Fluid Mechanical Investigations of Ciliary Propulsion," Ph.D. thesis, California Institute of Technology, Pasadena, CA.

[17] Blake, J. R., and Winet, H., 1980, "On the Mechanics of Muco-Ciliary Transport," Biorheology, **17**(1–2), pp. 125–134.

[18] Smith, D. J., Gaffney, E. A., and Blake, J. R., 2007, "A Viscoelastic Traction Layer Model of Muco-Ciliary Transport," Bull. Math. Biol., **69**, pp. 289–327.

[19] Ross, S. M., 1971, "A Wavy Wall Analytic Model of Muco-Ciliary Pumping," Ph.D. thesis, John Hopkins University, Baltimore, MD.

[20] Liron, N., and Rozenson, M., 1983, "Muco-Ciliary Transport," J. Submicrosc. Cytol., **15**(1), pp. 317–321.

[21] Mitran, S. M., 2007, "Metachronal Wave Formation in a Model of Pulmonary Cilia," Comput. Struct., **85**(11–14), pp. 763–774.

[22] Mitran, S. M., 2013, "Continuum-Kinetic-Microscopic Model of Lung Clearance Due to Core-Annular Fluid Entrainment," J. Comput. Phys., **244**, pp. 193–211.

[23] Lee, P. S., Gerrity, T. R., Hass, F. J., and Lourenco, R. V., 1979, "A Model for Tracheobronchial Clearance of Inhaled Particles," IEEE Trans. Biomed. Eng., **26**(11), pp. 624–630.

[24] Asgharian, B., Hofmann, W., and Miller, F. J., 2001, "Mucociliary Clearance of Insoluble Particles From the Tracheobronchial Airways of the Human Lung," J. Aerosol Sci., **32**(6), pp. 817–832.
[25] Hofmann, W., and Sturm, R., 2004, "Stochastic Model of Particle Clearance in Human Bronchial Airways," J. Aerosol Med., **17**(1), pp. 73–89.
[26] Farkas, A., and Szöke, I., 2013, "Simulation of Bronchial Mucociliary Clearance of Insoluble Particles by Computational Fluid and Particle Dynamics Methods," Inhalation Toxicol., **25**(10), pp. 593–605.
[27] Panton, R. L., 2013, *Incompressible Flow*, Wiley, New York.
[28] Button, B., Cai, L. H., Ehre, C., Kesimer, M., Hill, D. B., Sheehan, J. K., Boucher, R. C., and Rubinstein, M., 2012, "A Periciliary Brush Promotes the Lung Health by Separating the Mucus Layer From Airway Epithelia," Science, **337**(6097), pp. 937–941.
[29] Weibel, E. R., 1963, *Morphometry of the Human Lung*, Springer Verlag Academic, Berlin.
[30] Weibel, E. R., and Gomez, D. M., 1962, "Architecture of the Human Lung," Science, **137**(3530), pp. 577–585.
[31] Horsfield, L., Dart, G., Olson, D. R., Filley, G. F., and Cumming, G., 1971, "Models of the Human Bronchial Tree," J. Appl. Physiol., **31**(2), pp. 207–217.
[32] Garimella, R. V., and Swartz, B. K., 2003, "Curvature Estimation for Unstructured Triangulations of Surfaces," Technical Report, Los Alamos National Laboratory, Los Alamos, NM, Report No. LA-UR-03-8240.
[33] ICRP, 1994, "Human Respiratory Tract Model for Radiological Protection," International Commission on Radiological Protection (ICRP), Ottawa, ON, Canada, (ICRP) Publication 66.
[34] Matsui, H., Randell, S. H., Peretti, S. W., Davis, C. W., and Boucher, R. C., 1998, "Coordinated Clearance of Periciliary Liquid and Mucus From Airway Surfaces," J. Clin. Invest., **102**(6), pp. 1125–1131.
[35] Hofmann, W., Mènache, M. G., and Graham, R. C., 1993, "Radon Dosimetry in the Rat Lung," Health Phys., **64**(3), pp. 279–290.
[36] Knowles, M., and Boucher, R. C., 2002, "Mucus Clearance as a Primary Innate Defense Mechanism for Mammalian Airways," J. Clin. Invest., **109**(5), pp. 571–577.
[37] Majima, Y., 2002, "Mucoactive Medications and Airway Disease," Paediatr. Respir. Rev., **3**(2), pp. 104–109.
[38] Moriarty, J. A., and Grotberg, J. B., 1999, "Flow-Induced Instabilities of a Mucus-Serous Bilayer," J. Fluid Mech., **397**(1), pp. 1–22.
[39] Schurch, S., Gehr, P., Hof, V. I., Geiser, M., and Green, F., 1990, "Surfactant Displaces Particles Toward the Epithelium in Airways and Alveoli," Respir. Physiol. Neurobiol., **80**(1), pp. 17–32.
[40] Schürch, S., 1982, "Surface Tension at Low Lung Volumes: Dependence on Time and Alveolar Size," Respir. Physiol., **48**(3), pp. 339–355.
[41] Filoche, M., Tai, C. F., and Grotberg, J. B., 2015, "Three-Dimensional Model of Surfactant Replacement Therapy," Proc. Natl. Acad. Sci. U. S. A., **112**(30), pp. 9287–9292.
[42] Grotberg, J. B., Halpern, D., and Jensen, O. E., 1995, "Interaction of Exogenous and Endogenous Surfactant: Spreading-Rate Effects," J. Appl. Physiol., **78**(2), pp. 750–756.
[43] Bull, J. L., Nelson, L. K., Walsh, J. T., Glucksberg, M. R., Schurch, S., and Grotberg, J. B., 1999, "Surfactant-Spreading and Surface-Compression Disturbance on a Thin Viscous Film," ASME J. Biomech. Eng., **121**(1), pp. 89–98.
[44] Cassidy, K. J., Halpern, D., Ressler, B. G., and Grotberg, J. B., 1999, "Surfactant Effects in Model Airway Closure Experiments," J. Appl. Physiol., **87**(1), pp. 415–427.
[45] Foster, W. M., Langenback, E., and Bergofsky, E. H., 1980, "Measurement of Tracheal and Bronchial Mucus Velocities in Man: Relation to Lung Clearance," J. Appl. Physiol., **48**(6), pp. 965–971.